

The effect of aerosol on warm convective clouds: Aerosol-cloud-surface flux feedbacks in a new coupled large eddy model

Hongli Jiang¹ and Graham Feingold²

H. Jiang CIRA/NOAA Earth System Research Laboratory, Boulder, Colorado, 80305.
(Hongli.Jiang@noaa.gov)

G. Feingold NOAA Earth System Research Laboratory, 325 Broadway, Boulder, Colorado
80305. (Graham.Feingold@noaa.gov)

¹Cooperative Institute for Research in the
Atmosphere/NOAA Earth System Research
Laboratory, Boulder, CO 80305.

²NOAA Earth System Research Laboratory,
Boulder, CO 80305.

Abstract. We present a new large eddy simulation model that comprises coupled components representing size-resolved aerosol and cloud microphysics, radiative properties of aerosol and clouds, dynamics, and a surface soil and vegetation model. The model is used to investigate the effect of increases in aerosol on liquid water path LWP, cloud fraction, optical depth, and precipitation formation in warm, continental cumulus clouds. Sets of simulations that either neglect, or include the radiative properties of a partially absorbing aerosol are performed. In the absence of aerosol radiative effects, an increase in aerosol loading results in a reduction in precipitation however the clouds do not experience significant changes in LWP, cloud fraction and cloud depth; aerosol effects on LWP and cloud fraction are small compared to the dynamical variability of the clouds at any given aerosol concentration. Reasons for this response are discussed. When aerosol radiative effects are included, the modification in atmospheric heating profiles, and the reduction in surface latent and sensible heat fluxes resulting from the presence of these particles, have a significant effect on cloud parameters and boundary layer evolution. For the case considered, there is a significant reduction in the strength of convection, LWP, cloud fraction and cloud depth. Cloud optical depth responds non-monotonically to the increase in aerosol. These results indicate that in continental regions surface processes must be included in calculations of aerosol-cloud-precipitation interactions. Neglect of these surface processes may result in an overestimate of the second aerosol indirect effect.

1. Introduction

The aerosol-cloud-climate system is a complex one, comprising myriad feedbacks that challenge our ability to predict the radiative response of clouds to changes in aerosol. In addition to the direct effect of aerosol on radiation (the “direct effect”), a host of “aerosol indirect effects” have been proposed. These include the “first indirect effect” [Twomey, 1974] which considers the response of cloud drop size and reflectance to a change in aerosol with reference to a constant liquid water content (LWC); the “second indirect effect” [Albrecht, 1989] which proposes that an increase in aerosol will reduce the ability of a cloud to precipitate, increase cloud liquid water, and extend cloud coverage and lifetime; the “semi direct effect” [Grassl, 1975; Hansen *et al.*, 1997] that considers the reduction in cloudiness due to the presence of absorbing aerosol in the atmosphere; and various other indirect effects [e.g., Jacobson, 2002; Lohmann and Feichter, 2005] that await further elucidation.

The first indirect effect, or the closely related aerosol effect on cloud drop number and size, has been identified in numerous in-situ observations [Warner and Twomey, 1967; Durkee *et al.*, 2000; Brenguier *et al.*, 2000], by satellite remote sensors [Kaufman and Nakajima, 1993; Han *et al.*, 1998; Bréon *et al.*, 2002; Nakajima *et al.*, 2001] and surface-based remote sensors [e.g., Feingold *et al.*, 2003; Kim *et al.*, 2003] but quantification of the magnitude of this effect remains an elusive goal. This is illustrated by the range of observed relationships between cloud drop concentration N_d and accumulation mode aerosol concentration N_a derived from field studies [see, e.g., Ramanathan *et al.*, 2001]. The range of N_d vs. N_a relationships is due in varying, and uncertain degrees to aerosol concentration, size distribution, composition and updraft velocity [e.g., Twomey, 1959;

Leaitch et al. 1996; *Facchini et al.*, 1999; *Nenes et al.*, 2002; *Feingold*, 2003]. Improved understanding of the $N_d - N_a$ relationship is not a sufficient criterion for assessment of the first indirect effect, which must also include the effects of spatial heterogeneity and three-dimensional cloud structure.

The second indirect effect relaxes the reference to constant LWC and opens a very broad range of possibilities of cloud response to aerosol via dynamical, radiative, and even surface flux feedbacks. Observational assessments of the second indirect effect, including perturbations to cloud life-cycles, are very difficult to achieve, but there is evidence of aerosol-induced reduction in precipitation, particularly associated with biomass burning [*Warner*, 1968; *Rosenfeld*, 1999]. A number of modeling studies have pointed out that even the sign of these responses is unclear [*Stevens et al.*, 1998; *Jiang et al.*, 2002; *Feingold and Kreidenweis*, 2002] and dependent amongst others, on temperature, humidity and stability parameters, both in the boundary layer and above [*Ackerman et al.*, 2004; *Lu and Seinfeld*, 2005]. In the marine stratocumulus environment, increases in aerosol result in decreases in cloud liquid water path (LWP) when dry air resides above the boundary layer, whereas moister conditions above the boundary layer result in an increase in LWP with increasing aerosol [*Ackerman et al.*, 2004]. *Stevens et al.* [1998] showed that when the air above the stratocumulus-capped boundary layer is moist, a small amount of drizzle promotes higher LWP by stabilizing the boundary layer and reducing entrainment rates. *Jiang et al.* [2002] showed that polluted aerosol layers residing above stratocumulus clouds reduced precipitation as well as LWP by reducing the supply of moisture from cumulus penetrating into stratocumulus. In their simulations, cloud albedo was almost unaffected by the increases in aerosol because increases in drop number concentration

were accompanied by decreases in LWP. Such effects are likely highly sensitive to the thermodynamic state of the atmosphere.

The semi-direct effect introduces added feedbacks due to the radiative properties of the aerosol (i.e., the direct effect). During the daytime, absorbing aerosol heats the atmosphere locally and reduces the amount of solar radiation reaching the surface. These factors tend to stabilize the atmosphere and make it less conducive to convection [Grassl, 1975; Hansen *et al.*, 1997; Ackerman *et al.*, 2000; Koren *et al.*, 2004], although there is some dependence on the vertical distribution of the aerosol [Johnson *et al.*, 2004; Feingold *et al.*, 2005]. Over the land, the reduction in downwelling solar radiation, and associated decrease in surface latent and sensible heat fluxes, result in further, significant reduction in cloud fraction and LWP, regardless of the vertical distribution of the absorbing aerosol [Feingold *et al.*, 2005]. Finally, soil moisture, which is closely linked to latent heat flux and precipitation, is also known to be important in regulating aerosol-radiation-dynamical interactions [Yu *et al.*, 2002].

The goal of the current study is to extend our prior work by examining the effect of aerosol on warm cumulus clouds in a continental setting with a broad range of aerosol conditions. Feingold *et al.* [2005] considered coupled components of aerosol, cloud, dynamics, and radiation, but fixed the surface fluxes. The new model includes a coupled, interactive surface model and therefore allows (i) cloud drop number and size to respond to changes in aerosol; (ii) radiation and dynamics to respond to changes in cloud drop size; (iii) absorbing aerosol to affect radiation; and (iv) absorbing aerosol to affect surface latent and sensible fluxes. It will be shown that these feedbacks at the small-scale manifest themselves as a rather unpredictable system, whose evolution likely depends strongly on

the thermodynamic state of the atmosphere. This is consistent with the theme of recent studies on the second indirect, and semi-direct aerosol forcing of clouds.

2. Model Description

The model is a large eddy simulation based on the Regional Atmospheric Modeling System [RAMS, version 4.3, *Cotton et al.*, 2003] coupled to a microphysical model described by *Feingold et al.*, [2005]. The Land Ecosystem-Atmosphere Feedback (LEAF) model [*Walko et al.*, 2000] is incorporated into the model of *Feingold et al.* [2005] for the current study. The model has undergone extensive testing as part of the Global Energy and Water Cycle Experiment (GEWEX) Cloud System Study (GCSS) Boundary Layer Working Group intercomparison studies for stratocumulus, [e.g., *Stevens et al.*, 2004], trade-wind cumulus [*Siebesma et al.*, 2003], and convective cumulus over land [*Brown et al.*, 2002]. New aspects of the model not addressed in those intercomparisons will receive more scrutiny here. A brief description of each module is given below.

2.1. Bin Microphysical Model

Warm cloud processes including activation, condensation/evaporation, collision-coalescence, regeneration of particles upon complete evaporation of drops, and sedimentation are solved using the method of moments based on *Tzivion et al.* [1987]. Drop mass, drop number, as well as aerosol mass are accounted for in each drop bin [*Feingold et al.*, 1996]. The model includes a size-resolved representation of aerosol and cloud drops; aerosol are represented by 14 size-bins over the range $0.04\text{ }\mu\text{m}$; $7\text{ }\mu\text{m}$ (radius) with both mass and number calculated in each bin. Upon complete evaporation of droplets, particles are returned to the atmosphere in a manner that conserves number and mass

concentration. Aerosol growth processes are not simulated for these relatively short duration (8 h) simulations. In *Feingold et al.* [2005], only 12 drop size bins were required for the highly polluted conditions studied there. In the current version of the model, 33 size-bins covering the drop range 1.56 μm ; 2.54 mm (radius) are needed to simulate growth to precipitation-sized drops. This configuration requires prognostic equations for 128 scalars.

Kelvin and solute corrections to the supersaturation field experienced by droplets are also included and coupled to the condensation/evaporation equation and the equation for prediction of supersaturation following *Harrington et al.* [2000]. These terms can become important at extremely large aerosol concentrations, and/or very low updrafts when cloud supersaturation is low; it should be noted, however, that under high aerosol loadings, the microphysical details of smoke aerosol transition to droplets can be better resolved with a Lagrangian parcel model [*Feingold et al.*, 2001]. The strength of the current model is that it strives to represent the various dynamical, microphysical, radiative, and surface components (as described below) with reasonable balance.

2.2. Radiative Properties of Clouds and Aerosol

The model's 8-band coupled radiation model [*Harrington et al.* 2000] was originally formulated to simulate radiative effects of cloud drops and was coupled to the bin microphysical scheme described above. In the current work, the direct radiative effect of aerosol is included [*Feingold et al.* 2005]. Aerosol size distributions are initialized as log-normal distributions ($r_g = 0.1 \mu\text{m}$ and $\sigma = 1.5$) with a range of concentrations [Table 1]. Aerosol particles are assumed to consist of an internal mix of soot and ammonium sulfate. Their optical properties (extinction, single scattering albedo ω_o , and phase function) are

calculated based on this mix, and the ambient relative humidity. Off-line calculations of these optical properties are performed a priori and stored for access during simulations. For the case to be presented ω_o is about 0.90 at a wavelength of $0.47 \mu\text{m}$, but a purely scattering aerosol is also considered. Particles are assumed to be at equilibrium with their environment, except for particles $> 0.1 \mu\text{m}$ which are at 0.97 of their equilibrium sizes. Heating rates associated with smoke aerosol embedded inside droplets are calculated based on *Conant et al.* [2002] and coupled to the condensation/evaporation equation and the equation for prediction of supersaturation following *Harrington et al.* [2000].

All simulations described below include coupling of the cloud drop-radiation interactions, but the direct effect is alternately included or neglected to assess its importance.

2.3. Leaf Model

The LEAF model represents the storage and exchange of energy (heat and moisture) fluxes between the surface and atmosphere. Four processes are considered when evaluating the latent heat fluxes. They are the transpiration through the stomata on plants, evaporation from the soil, and evaporation and condensation of moisture on the vegetation. A version of the TOP-MODEL [*Band, 1993*], a land hydrology model, is coupled to the LEAF model to represent the subgrid-scale run-off. In the LEAF model, vegetation may be multilayered in terms of leaf area index, but is represented by a single prognostic temperature and surface moisture. There are 12 soil types and 18 vegetation types from which to select. Each individual grid column can be assigned to either a single type, or a mosaic of different types. A sandy clay loam for the soil texture, and evergreen broad leaf for the vegetation are chosen for this study, and applied over the entire domain. There are 8 soil layers with a root depth of 0.4 m. The leaf area index is 6.

The initial volumetric soil moisture content used in the model is $0.22 \text{ m}^3 \text{ m}^{-3}$ corresponding to a relative wetness of 52% at the saturation content of $0.42 \text{ m}^3 \text{ m}^{-3}$. This compares well with the average soil moisture content of $0.2 - 0.3 \text{ m}^3 \text{ m}^{-3}$ observed by *Alvala et al.* [2002] for the month of September 1999 at Fazenda.

Longwave radiation is emitted, absorbed, and reflected by soil and vegetation, while downward solar (shortwave) radiation is absorbed by soil and vegetation. Changes in temperature and heat fluxes due to absorption and reflection of radiation are calculated in the LEAF model.

All simulations described below include the interactive LEAF model. The reader is referred to *Feingold et al.* [2005] for simulations of the same case with imposed diurnally varying fluxes.

2.4. Validation of the coupled model

Although the coupled surface model has been validated in prior studies [e.g., *Golaz et al.* 2001] a test of this coupling is shown in Figure 1a for one of the simulations to be described below (S1; Table 1). The net surface radiation [$R_{net} = (S^\downarrow - S^\uparrow) + (L^\downarrow - L^\uparrow)$, where S indicates shortwave, L indicates longwave, and the superscripts \downarrow and \uparrow represent incoming and outgoing components] is plotted together with the sum of surface latent and sensible heat fluxes. The good agreement between these fields shows that the surface model is responding correctly to changes in the net radiation. The small difference in the fields (about 20 W m^{-2} and consistent with *von Randow et al.*, 2004) is the ground storage term. Measurements of the diurnal cycle of R_{net} for the dry season at Fazenda [*von Randow et al.* 2004] show peak noontime (LT) values of about 720 W m^{-2} , almost identical to the simulated values in Figure 1.

Figure 1b separates the total surface flux in Figure 1a into its sensible and latent heat flux components. The mean Bowen ratio over the period 08:00 h to 16:00 h local time (LT) is 0.30. Late September coincides with the end of the dry season and observations of the sensible heat flux [*Fisch et al.* 2004] show maximum daytime fluxes of $\sim 200 \text{ W m}^{-2}$ - comparable to the modeled surface sensible heat flux in Figure 1b. The observed daily mean Bowen ratios at the pasture site for September/October are ~ 0.50 [*von Randow et al.* 2004], i.e., somewhat larger than the mean value of 0.30 averaged over 08:00 to 16:00 LT from Figure 1b. The disparity can be explained by the assumption of an evergreen broadleaf vegetation model rather than the pasture; Evergreen broadleaf has a smaller albedo, larger vegetation fraction, larger leaf area index, and deeper roots than pasture. Thus the simulations tend to have higher latent heat fluxes than observed seasonally averaged values. Other sources of the disparity may be due to the fact that the observations are monthly averages, as well as differences in the period of the day included in the averaging.

3. Initial Conditions and Experiment Design

Following *Feingold et al.* [2005], simulations are based on a sounding on 26 September, 2002 at 07:38 LT (11:38 UTC) from a continental site in Brazil (Fazenda) during the Smoke Aerosols, Clouds, Rainfall and Climate (SMOCC) experiment [*Andreae et al.* 2004]. Fazenda is a pasture site located at $10^\circ 45' \text{ S}$ and $62^\circ 21' \text{ W}$ at an altitude of 290 m above sea level. Although the simulations to be presented are not intended as a rigorous case study, it will be shown that the simulated fields are in broad agreement with observations. The sounding was chosen because it generates convective cumulus clouds that do not produce ice, and allows for testing of the effects of varying amounts of aerosol on

warm cumulus clouds. The initial potential temperature (θ) sounding used as input to the model is a slightly modified form of the actual sounding (Figure 2) with some stabilization added above ~ 3000 m to prevent clouds growing too deep. The initial water vapor field (not shown) is the same as the measured profile with some drying above 3000 m. The observed and simulated θ soundings at 14:00 LT are in good agreement and represent the deepening continental boundary layer as the day progresses.

The simulations are performed for a little over 8 h (500 min). The domain size is 6 km \times 6 km \times 5 km with $\Delta x = \Delta y = 100$ m and $\Delta z = 50$ m. The time step is 2 s. Two sets of three-dimensional simulations were performed, as summarized in Table 1. Each set consists of four simulations with aerosol concentrations of 100, 500, 1000, and 2000 cm^{-3} . Set 1 (S1) treats the aerosol as cloud condensation nuclei CCN, but the aerosol and radiation modules are not directly coupled. (Indirect coupling occurs only through cloud microphysical-radiation interactions.) Set 2 (S2) also includes the direct coupling of aerosol heating with the dynamical model. All simulations have an initial aerosol profile that is invariant with height, chosen so as to avoid the radiative-dynamic feedback associated with vertical structure in the aerosol, as described in *Feingold et al.* [2005]. There it was found that aerosol layering could influence convection and cloud response to aerosol [see also *Johnson et al.*, 2004]. This constant profile tends to produce aerosol optical depths that are higher than implied by the number concentrations alone, but as will be seen, inferences for lower optical depths can easily be made by scaling results over the range of clean and polluted conditions.

4. Simulation Results

We present selected time-series and mean profiles of different cloud properties averaged over the horizontal ($x-y$) plane (referred to as layer averages), and then time-averaged either over one hour, or over several hours during the course of the simulations. Comparison between set 1 (S1) simulations will be presented first to show the response of the boundary layer clouds to changes in aerosol concentrations without inclusion of aerosol-dynamical feedbacks. This is followed by presentation of set 2 (S2) results and a comparison to S1.

4.1. Time series

4.1.1. S1: No direct effects.

Figure 3 presents, for S1 simulations, time-series of liquid water path, LWP (averaged only over columns that have LWP greater than 20 g m^{-2}), cloud fraction (the fraction of grid points that have cloud water $r_c > 0.01 \text{ g kg}^{-1}$), cloud depth (Z_{depth}), cloud base, surface drizzle rate (F_{driz} , averaged over points with values $\geq 0.1 \text{ mm day}^{-1}$), vertically integrated number concentration of droplets ($N_{d,int}$), and cloud optical depth (τ_c , averaged over all cloudy regions with $\tau_c > 2$) for three of the four initial aerosol concentrations. The results of S1-1000 are not plotted in Figure 3 to enhance the clarity of presentation; they will be considered in subsequent figures. The simulated cloud base is in general agreement with the observed cloud base of 1875 m at 14:00 LT (based on the flight log). Note that in calculating cloud fraction, cloud top, base, and depth, it was found that robust results were obtained using either a r_c (drops $< 25 \mu\text{m}$ radius) threshold of 0.01 g kg^{-1} , or a criterion that the ratio of total mixing ratio (the sum of the vapor and water mixing ratios) to the saturation mixing ratio at the local temperature be ≥ 1 . The $r_c > 0.01 \text{ g kg}^{-1}$ criterion is used throughout. When the sum of all water bins ($r_l = \text{cloud} +$

rain) was used as a criterion, cloud fraction and cloud boundaries were biased by subcloud precipitation.

The time series of LWP (Figure 3a) show no clear dependence on N_a over the range $100 \text{ cm}^{-3} \leq N_a \leq 2000 \text{ cm}^{-3}$ although the increase in aerosol does change the frequency and duration of cloud events. The time series has a number of distinct maxima that are correlated with higher cloud fraction and a deeper cloud layer. The increase in N_a results in higher $N_{a,int}$ (Figure 3f). Surface drizzle events occur only when clouds grow deep enough ($\sim 700 \text{ m}$, Figure 3e), LWP exceeds about 400 g m^{-2} , and then only for the cleaner cases ($N_a = 100, 500 \text{ cm}^{-3}$). As expected, surface rain (Figure 3d) is suppressed for the polluted cases ($N_a = 2000 \text{ cm}^{-3}$) because of a reduction in the growth of drops via collision-coalescence [e.g., *Warner*, 1968].

A sample of fields presented in Figure 3 are now time-averaged over the last 5 h (11 h to 16 h LT) and plotted as a function of N_a (Figure 4). The mean and standard deviation of each field is shown. As N_a increases from 100 cm^{-3} to 2000 cm^{-3} the cloud-averaged LWP is approximately constant whereas the domain-averaged LWP decreases (Figures 4a,d). Superimposed on Figures 4a,d are calculations of the LWP calculated from cloud droplets alone (radius $r \leq 25 \mu\text{m}$) for the simulations at $N_a = 100 \text{ cm}^{-3}$, 500 cm^{-3} and 1000 cm^{-3} . It can be seen that precipitation-sized drops contribute significantly to the LWP under clean conditions and that an increase in N_a from 100 cm^{-3} to 500 cm^{-3} does result in an increase in LWP (based on r_c only). The % increase is approximately the same for the cloud-averaged and domain-averaged LWP calculations. The differences between the two LWP calculations diminish rapidly with increasing N_a and decreasing precipitation.

Thus the inclusion of all drop sizes in the LWP calculation tends to remove the positive correlation between N_a and LWP.

Cloud fraction and cloud depth are relatively unaffected by the aerosol (Figure 4b,c) although cloud fraction does tend to decrease with increasing aerosol. Vertically integrated droplet concentrations $N_{d,int}$ calculated for cloudy regions only (Figure 4e) increase from $41 \times 10^4 \text{ cm}^{-2}$ to $831 \times 10^4 \text{ cm}^{-2}$. Figure 4f shows two calculations of the cloud optical depth (visible wavelength): the first (solid line) is an average over cloudy regions ($\tau_c > 2$) and the second (dashed line) is a domain average. In the first case, τ_c increases from 11 to about 26, while in the latter the increase is from 2 to 4, commensurate with the low cloud fractions. Of note is the fact that except for drop concentration and τ_c , the dynamical variability in the fields at any given aerosol concentration is much greater than the effect due to changes in aerosol.

4.1.2. S2: Aerosol-Radiative Coupling.

As in Figure 3, time series of the various fields for S2 simulations are shown in Figure 5. Here, LWP, cloud fraction, cloud depth, and cloud base show distinct decreases with increasing aerosol amounts (Figures 5a-d), particularly when comparing results for $N_a = 100 \text{ cm}^{-3}$ and $N_a = 2000 \text{ cm}^{-3}$. Precipitation is now suppressed at $N_a \geq 500 \text{ cm}^{-3}$. $N_{d,int}$ variability is similar to that in Figure 3f so instead the domain-maximum $\langle w'w' \rangle$ (averaged over the horizontal plane), a measure of the strength of convection, is plotted. Figure 5g shows total surface heat flux ($F_{sen+lat}$, the sum of the surface sensible and latent heat fluxes). It is seen that the increase in N_a tends to decrease convective activity and surface fluxes.

As in Figure 4, 5-h time-averaged fields are shown in Figure 6 and calculations from S1 simulations (without standard deviations) are superimposed for comparison. In addition to the fields shown in Figure 4, the surface air temperature (T_{sfc}), net surface radiative flux (R_{net}), and $F_{sen+lat}$ are also shown. Note that the aerosol effect on LW radiation is negligible; nevertheless R_{net} is plotted for energy balance considerations. Table 2 (see below) focuses on SW fluxes alone.

The general tendencies with respect to increases in N_a are quite different from those in S1. In the mean, when N_a increases from 100 cm^{-3} to 2000 cm^{-3} , the cloud-averaged LWP decreases by 64% (Figure 6a); cloud fraction decreases by 58% (Figure 6b); and cloud depth decreases by 62% (Figure 6d) (all calculations relative to S2-100), although there is still a great deal of dynamical variability at any given N_a . The increase in N_a leads to a smaller increase in the vertically integrated $N_{d,int}$ ranging from $40 \times 10^4 \text{ cm}^{-2}$ to $540 \times 10^4 \text{ cm}^{-2}$; activated fractions are smaller than in S1 due to reduced convective activity associated with the suppressed surface fluxes (Figures 5f,g and 6h). The smaller increase in $N_{d,int}$ and larger decrease in LWP result in an increase in cloud optical depth from S2-100 to S2-500, and then a decrease back to roughly the same value as S2-100. The clouds become optically thinner above $N_a = 500 \text{ cm}^{-3}$, largely because of the decreasing cloud depth and LWP.

In the S1 simulations, as N_a increases from 100 cm^{-3} to 2000 cm^{-3} the surface air temperature is unchanged (values are within 0.04°C of each other; Figure 6f); the net radiative flux at the surface decreases by only 2.2% (Figure 6g); changes in surface total heat flux are almost the same (Figure 6h) to balance the decrease in R_{net} . In these S1 simulations, the R_{net} and $F_{sen+lat}$ are reduced only slightly by the increase in N_a over the

5 h time period because the aerosol is not coupled to the dynamical model. Any effects are due to the change in cloud microphysical properties (section 5.2).

Decreases in R_{net} (Figure 6g) relative to S1 range from 8% for the clean (S2-100) to a maximum of 31% for the polluted (S2-2000) case. The commensurate reduction in the surface total heat flux (Figure 6h) leads to a maximum of 1.32°C surface cooling relative to the S1 simulation for the most polluted conditions (Figure 6f).

Table 2 presents calculations of upwelling shortwave (SW) fluxes at the top of the atmosphere (TOA) and downwelling SW fluxes at the surface. In the S2 simulations, the absorption and scattering of aerosols block up to 26.5 % of the solar radiation from reaching the surface. For the clean case (S2-100), the absolute amount of reduction in downwelling SW fluxes at the surface is balanced by the increase in the reflection of solar radiative flux back to space at TOA. The reflection at TOA is similar for all cases.

The clean case, S2-100, has a relatively low $\tau_{a,dry} = 0.04$ (Table 1) and aerosol heating contributes very little to the microphysical fields. The ratio of τ_a (Table 1, $N_a = 100 \text{ cm}^{-3}$) to domain-averaged cloud optical depth τ_c (Figure 6e) is only 2.1%. The results corresponding to $N_a = 100 \text{ cm}^{-3}$ are therefore statistically the same as those in S1-100 for the fields plotted in Figure 6a – 6e. Comparison of the time series between the S1-100 and S2-100 (e.g. Figures 3a and 5a) reveals that although the temporal averaging shows no significant difference, the two cases evolve at different frequencies. The higher surface fluxes in S1-100 are responsible for clouds with higher LWP developing earlier than in S2-100, but dynamical feedbacks due to precipitation (e.g., the strong precipitation event between 13 h and 14 h in Figure 3e) prevent the fields diverging in a statistical sense.

Therefore, on average, the small reduction in R_{net} and $F_{sen+lat}$ at the surface does not manifest itself in changes in parameters associated with cloud evolution.

4.2. Vertical profiles

4.2.1. No aerosol-dynamical coupling.

Profiles of cloud drop concentration N_d , rainrate F_{driz} , drop effective radius r_{eff} , and mixing ratio r_l (all drops), time-averaged over the last 5 h of simulations, 11 – 16 LT are shown in Figure 7. All profiles are domain-averages, except for r_{eff} , which is averaged over cloudy regions. These profiles require some caution in their interpretation. They should not be interpreted in the manner that all clouds have bases of ~ 1500 m and tops of ~ 4500 m. Rather, clouds with different depths are formed over this height range. A strong positive correlation between N_a and N_d , and a negative correlation with r_{eff} are clearly evident. In the most polluted case ($N_a = 2000 \text{ cm}^{-3}$), the maximum in-cloud r_{eff} is only $9.5 \mu\text{m}$. This is much smaller than the value of $14 \mu\text{m}$ sometimes considered to be a precipitation threshold radius [Rosenfeld, 1999]. Although the maximum r_{eff} for the S1-1000 simulation is approximately $14 \mu\text{m}$, there is no indication of surface precipitation in the mean profile (Figure 7c). In the clean case ($N_a = 100 \text{ cm}^{-3}$), the average r_{eff} is as high as $80 \mu\text{m}$ in the cloud layer and about $180 \mu\text{m}$ as rain falls below the cloud base; drizzle rates are commensurate (Figure 7c).

The reduction in LWP with increasing aerosol concentration derived from integration of the r_l profiles in Figure 7d ($\text{LWP} = \Sigma \rho r_l \Delta z$, where ρ is the air density) is consistent with Figure 4d (including all water; solid line). The reason for this reduction lies partially in the fact that on average cloud fraction tends to decrease with increasing N_a (Figure

4b). It is also partially due to the larger relative contribution of precipitating drops to r_l for clean cases.

Figure 7d therefore makes the important point that although the LWP averaged over cloudy columns may not be sensitive to increases in aerosol, the domain-averaged LWP may show a different response if the cloud fraction changes (in this case decreases) with increasing aerosol.

4.2.2. Aerosol-Dynamical feedbacks.

A figure similar to Figure 7 is plotted for S2 results (Figure 8). The most striking differences between the S1 and S2 profiles is manifested in r_l for all the cases, and r_{eff} and the drizzle rate for the S2-500 case. The S1-100 and S2-100 r_l profiles are quite similar, as expected, however, the S2 simulations now exhibit a much stronger decrease in r_l with increasing N_a . For S2-500, r_{eff} is only a third of that in S1-500 in the cloud layer, and the drizzle r_{eff} is reduced to about 10 μm at the surface. Drizzle barely reaches the surface because of the lower liquid water environment. In other words, the reduced liquid water is insufficient to generate drizzle at these cloud drop concentrations.

The direct effect of aerosol clearly has a significant effect on cloud evolution in this coupled system. First and foremost, increases in N_a (or τ_a) block solar radiative flux from reaching the surface; second, increases in N_d associated with the increases in N_a result in optically thicker clouds that block solar radiative flux even further. The reduced surface radiative flux results in reduced $F_{sen+lat}$, which acts to reduce convection and cloud amount. In addition, the aerosol heating contributes to further reductions in cloud liquid water through stabilization of the sub-cloud layer [e.g., *Feingold et al.*, 2005]; there is about 1 K day⁻¹ difference in solar heating rates below cloud, and 2.5 K day⁻¹ at about

3000 m in the cloud layer, between the clean (S2-100) and the most polluted simulations (S2-2000) (Figure 9b). (The solar heating rates are almost identical amongst the S1 simulations; Figure 9a.) The longwave heating rates for both S1 and S2 (not shown) are approximately -2 K day^{-1} with negligible sensitivity to aerosol concentration.

Note that aerosol heating inside the droplets is simulated but as discussed in *Feingold et al.* [2005], this effect is negligible compared to the effects of reduced surface fluxes and stabilization.

4.2.3. Single scattering albedo. All the S2 results presented above are performed using a single scattering albedo $\omega_0=0.9$. One additional S2 simulation with $N_a = 1000 \text{ cm}^{-3}$ was performed for pure scattering ($\omega_0 = 1.0$). Table 3 lists several fields that are time-averaged over the last 5 h of the simulation, a comparison of S2-1000 ($\omega_0=0.9$) and S2-1000 ($\omega_0 = 1.0$), and differences between the two simulations. Absorption reduces the surface radiative flux by 20.5 W m^{-2} , surface heat flux by 22.1 W m^{-2} , LWP by 36.7 g m^{-2} , and cloud cover by 0.027 relative to the $\omega_0 = 1.0$ case. Percentage differences are given in Table 3.

5. Discussion

Two sets of results have been shown. The first set (S1) examines how the boundary layer structure and cloud fields respond as the aerosol concentration N_a increases from clean to polluted conditions. The aerosol act only as CCN and their direct radiative effects are not coupled to the model dynamics. The second set of simulations (S2) is identical, except that aerosol radiative effects contribute to absorbing and scattering, and these effects are coupled to the dynamics.

5.1. Effect of N_a on LWP and precipitation

The results for the S1 simulations show some subtle but important differences from the hypothesis that an increase in N_d results in clouds with higher LWP and cloud fraction as a consequence of reduced precipitation (the second indirect effect). Although some weak trends appear to be due to aerosol, the dynamical variability in LWP and cloud fraction at any given N_a is much greater than the aerosol-induced change in LWP. The suppression of precipitation does not lead to a distinct increase in LWP (an average of cloudy columns) if all drop sizes are included in the LWP calculation (Figure 4a). On average, LWP does increase with increasing N_a when the precipitating drops are removed from the LWP calculations (Figure 4a). There is even some suggestion of a decrease in cloud fraction with increasing N_a which runs counter to the accepted hypothesis, possibly due to the fact that under polluted conditions, the more numerous, smaller droplets evaporate more efficiently because they present a larger surface area to volume ratio (*ceteris paribus*). For example, the characteristic evaporation timescale is $\propto (N_d \bar{r})^{-1}$ where \bar{r} is the mean drop radius [Squires, 1952]; a rough calculation suggests that this timescale is about 5 – 10 times faster for the polluted clouds than the clean clouds. Thus although the amount of water contained in cloud droplets ($r < 25 \mu\text{m}$) may increase with increasing N_a , their smaller size makes them more susceptible to evaporation at cloud edges. This subject is explored further in Xue and Feingold [2005].

We remind the reader that the concept of the second indirect effect [Albrecht, 1989] derives from one-dimensional turbulence closure model simulations of marine boundary layer clouds, and that those model simulations did not include explicit treatment of microphysical processes. Recent three-dimensional model results [Ackerman *et al.*, 2004; Lu

and Seinfeld, 2005] have shown that LWP may increase or decrease in the stratocumulus regime, depending on the thermodynamic profile. The current study suggests that the response may also be more complex in warm, continental cumulus clouds.

We note that in the cumulus cloud regime considered here, cloud fractions are only about 10% to 15% so that the potential for microphysical-dynamical feedbacks (e.g., through precipitation) is reduced to a much smaller area of the atmosphere than in the case of solid stratocumulus. Precipitation in the cleaner cases (S1-100 or S2-100) can affect cloud development by cooling and stabilizing the sub-cloud layer as evidenced in Figures 3 and 5. For example, there is a distinct decrease in LWP at 14:00 LT following a rain event with a rainrate of 100 mm d^{-1} (4 mm h^{-1}) at $\sim 13:30$ LT. In Figure 5 (S2 simulations), the absence of a strong difference in $\langle w'w' \rangle$ between S2-100 and S2-500 is a direct result of precipitation events beginning at 12:30 LT. Precipitation events tend to be followed by periods of significant reduction in $\langle w'w' \rangle$ (Figures 5e,f). Smaller amounts of rain have more limited impact on boundary layer development because of the relatively small cloud cover and the fact that only some fraction of clouds precipitate.

Thus for S2 simulations, there are two competing factors at work: first, convective activity tends to increase with increasing N_a as stabilization due to precipitation progressively diminishes; second, convective activity decreases with increasing N_a as surface fluxes are reduced. On average, the cleaner clouds do tend to be characterized by stronger convection.

5.2. N_a , N_d , and τ_c

As expected, Figure 3 shows that $N_{d,int}$ increases in response to the increase in N_a . $N_{d,int}$ and τ_c follow cycles that are correlated with the LWP, cloud fraction, and Z_{depth}

fields. Some of these correlations are quantified in Table 4. $N_{d,int}$ time series are clearly separated between the different N_a simulations. The separation is also quite distinct for the τ_c calculations, with exceptions occurring when clean clouds (S1-100) generate significantly more condensed water than their polluted counterparts (e.g. at $\sim 11:30$ and $13:50$ LT; Figure 3a).

The correlations between N_a , N_d , and τ_c (S1) are clear and robust after time averaging (Figure 4, Table 4) even though LWP is not necessarily constant. The effect of increasing N_a on the net radiative flux and the heat flux at the surface is small for the S1 simulations (Figure 6h), in spite of the doubling in τ_c from clean to polluted cases, because of the small cloud fractions.

In contrast, an increase in N_a causes significant reduction in surface fluxes in the S2 simulations, primarily due to the increase in τ_a , whose effects are felt over the entire surface. The reduction in LWP and cloud fraction with increasing N_a does little to reverse this trend because of the small cloud fractions. When the aerosol particles are allowed to contribute to heating, the 26.5% reduction in the downwelling radiative flux at the surface between S2-2000 and S2-100 (Table 2) is balanced by the reduction in the surface heat flux, which in turn results in further reduction in LWP, cloud fraction, cloud depth, and τ_c . These include the changes caused by increasing N_a that were visible in S1.

5.3. The Semi-direct Effect

The S2 simulations include both the effects of sub-cloud stabilization (warming of the atmosphere and cooling of the surface, Figures 9 and 6f) as well as the reduction in the surface sensible and latent heat fluxes. The simulations presented in *Feingold et al.* [2005] showed that the reduction in surface fluxes was sufficient by itself to explain the reduction

in cloud fraction. In that study, which used the same atmospheric sounding as used here, reduction in cloud fraction associated with sub-cloud boundary layer stabilization was shown to be less significant than that associated with changes in the surface fluxes. However, further work is required to quantify the relative importance of these factors for a range of thermodynamic and aerosol conditions.

6. Summary

We have presented results from two sets of large-eddy simulations (LES) of the 26 September 2002 Smoke, Aerosols, Clouds, Rainfall, and Climate [*Andreae et al.*, 2004] continental, warm cumulus cloud case. To avoid possible feedbacks associated with vertical layering of the aerosol, the initial aerosol profiles are assumed constant, and a range of aerosols concentrations are prescribed. The aerosol particles act only as CCN in set 1 (S1), while they also contribute to radiative-dynamical feedbacks in set 2 (S2).

The major results of this study may be summarized as follows:

For the S1 simulations:

- Increases in N_a in these warm cumulus clouds do not cause statistically significant changes in cloud fraction, LWP and cloud depth. There is even a small trend for cloud fraction to decrease with increasing N_a . Aerosol effects are well within the dynamical variability in LWP and cloud fraction at any given N_a . LWP is only shown to increase with N_a when droplets with radius $> 25 \mu\text{m}$ are excluded from the LWP calculation.

- Aerosol effects on N_d and τ_c are much more pronounced; increases in N_a result in increases in N_d and cloud optical depth τ_c . Correlation between N_d and τ_c is modulated by the high variability in the LWP field but in general τ_c correlates well with N_d (0.71 – 0.86; Table 4).

- As expected, increases in N_a are associated with decreases in effective radius and reductions in surface precipitation. In these simulations, The suppression of precipitation derives from the decrease in droplet sizes (less efficient collision-coalescence). The weak response of LWP to N_a does not modify this effect significantly.

For the S2 simulations (including aerosol direct effect-dynamical coupling):

The trends in the S2 results are quite different from those in S1, with evidence of strong decreases in LWP, cloud fraction, and cloud depth with increasing N_a associated with weaker convection. Aerosol effects on LWP induced by direct effects (stabilization and reduction in surface fluxes) are significant and much greater than those due to aerosol-cloud interactions in the absence of direct effects (Figure 6a).

The biggest difference between the S2 and S1 simulations derives from the fact that the direct effect blocks up to 26.5 % of incoming solar radiative flux from reaching the surface (for the most polluted case). The reduction in the surface radiative flux leads to a reduction in the surface heat flux and consequently weaker convection, much shallower clouds and lower cloud cover than in S1 simulations. The stabilization of the boundary layer due to surface cooling and aerosol heating aloft contributes to further reduction in convective activity. Stabilization due to precipitation in the clean case (S2-100) counters this to some extent so that differences between S2-100 and S2-500 are not as distinct as those between S2-500 and S2-2000. (Figure 5f).

Other points worth noting include:

- Cloud optical depth shows non-monotonic behavior as aerosol loadings increase due to the opposing effects of a decreasing drop size (which increases τ_c) and a decreasing

LWP (which decreases τ_c). With progressively higher N_a , a point is reached where the decrease in LWP dominates. In these simulations, this point occurs at $N_a \simeq 500 \text{ cm}^{-3}$.

- The effect of aerosol on the coupled cloud system is sensitive to the single scattering albedo of the aerosol. A change in ω_o from 1.0 to 0.9 causes reductions in temporally-averaged cloud fields of between ~ 10 and ~ 20 % (*ceteris paribus*).

This study has challenged us to look at some fundamental issues regarding aerosol-cloud-radiative-surface flux feedbacks in the cumulus cloud regime over land. In particular the sign of the change of aerosol induced effects on LWP and cloud fraction is called into question by this, and other recent studies. The study has also pointed to the importance of coupling aerosol radiative properties and a surface soil and vegetation model to the microphysical-dynamical model. As shown here, under polluted conditions (associated, e.g., with biomass burning smoke), the surface flux response to the aerosol may be the single most important factor in cloud reduction.

We stress that the results for the current study pertain to a single sounding, vegetation type and soil moisture, and we make no claims on the generality of the negligible microphysical effect of N_a on LWP, and the negative correlation between N_a and LWP when aerosol direct effects are simulated. Nevertheless, even in situations where this correlation is positive, neglect of the treatment of the associated reductions in surface fluxes will result in an overestimate of the response of LWP to aerosol, and its associated radiative cooling. Future work will attempt to delineate conditions under which negative and positive correlations between these parameters can be expected.

Acknowledgments. The authors thank NOAA's Climate Goal and NASA's IDS and Radiation programs for supporting this study. Helpful discussions with Robert Walko are acknowledged. We thank the reviewers for important comments.

References

- Ackerman, A. S., O. B. Toon, D. E. Stevens, A. J. Heymsfield, V. Ramanathan, and E.J. Welton, Reduction of tropical cloudiness by soot, *Science*, *288*, 1042–1047, 2000.
- Ackerman, A. S., M. P. Kirkpatrick, D. E. Stevens, and O. B. Toon, The impact of humidity above stratiform clouds on indirect aerosol climate forcing, *Nature*, *432*, 1014–1017, 2004.
- Albrecht, B. A., Aerosols, cloud microphysics, and fractional cloudiness, *Science*, *245*, 1227–1230, 1989.
- Alvalá, R. C. S., R. Gielow, H. R. da Rocha, H. C. Freitas, J. M. Lopes, A. O. Manzi, C. von Randow, M. A. F. S. Dias, O. M. R. Cabral, Intradiurnal and seasonal variability of soil temperature, heat flux, soil moisture content, and thermal properties under forest and pasture in Rodonia, *J. Geophys. Res.* *107*, 8043, doi:10.1029/2001JD000599, 2002.
- Andreae, M. O., Rosenfeld, D., Artaxo, P., Costa, A. A., Frank, G. P., Longo, K. M., Silva-Dias, M. A. F, Smoking rain clouds over the Amazon. *Science*, *303*, 1337–1342, 2004.
- Band, L. E., Effect of land surface representation on forest water and carbon budgets. *J. Hydrol.*, *150*, 749–772, 1993.
- Brenguier J.-L., and 9 coauthors, An overview of the ACE-2 CLOUDYCOLUMN closure experiment, *Tellus*, *52B*, 815–827, 2000.
- Bréon. F.-M., D. Tanré, and S. Generoso, Aerosol effect on cloud droplet size monitored from satellite, *Science*, *295*, 834–838, 2002.
- Brown, A. R., and co-authors, Large-eddy simulation of the diurnal cycle of shallow cumulus convection over land. *Quart. J. Roy. Meteor. Soc.*, *128*, 1075–1094, 2002.

- Conant, W.C., A. Nenes, and J. H. Seinfeld, Black carbon radiative heating effects on cloud microphysics and implications for the aerosol indirect effect. I. Extended Köhler theory, *J. Geophys. Res.* *107*, 4604, doi:10.1029/2002JD002094, 2002.
- Cotton, W. R., R. A. Pielke Sr., R. L. Walko, G.E. Liston, C.J. Tremback, H. Jiang, R.L. McAnelly, J.Y. Harrington, M.E. Nicholls, G.G. Carrio, and J. P. McFadden, RAMS 2001: Current status and future directions. *Meteorol. Atmos. Phys.*, doi:10.1007/s00703-001-0584-9, 2003.
- Durkee, P. A., K. K. Noone, and R. T. Bluth, The Monterey Area Ship Track Experiment, *J. Atmos. Sci.*, *57*, 2523–2541, 2000.
- Facchini, M. C., M. Mircea, S. Fuzzi, and R. J. Charlson, Cloud albedo enhancement by surface-active organic solutes in growing droplets, *Nature*, *401*, 257–259, 1999.
- Feingold, G., S. M. Kreidenweis, B. Stevens, and W. R. Cotton, Numerical simulation of stratocumulus processing of cloud condensation nuclei through collision-coalescence. *J. Geophys. Res.*, *101*, 21,391–21,402, 1996.
- Feingold, G., H. Jiang, and J. Y. Harrington, On smoke suppression of clouds in Amazonia, *Geophys. Res. Lett.* *32*, L02804, 10.1029/2004GL021369, 2005.
- Feingold, G., and S. M. Kreidenweis, Cloud processing of aerosol as modeled by a large eddy simulation with coupled microphysics and aqueous chemistry. *J. Geophys. Res.*, *107*, D23, 4687, doi:10.1029/2002JD002054, 2002.
- Feingold, G., W. L. Eberhard. D. E. Veron, and M. Previdi, First measurements of the Twomey aerosol indirect effect using ground-based remote sensors, *Geophys. Res. Lett.*, *30*, No. 6, 1287, doi:10.1029/2002GL016633, 2003.

- Feingold, G., Modeling of the first indirect effect: Analysis of measurement requirements, *Geophys. Res. Lett.*, *30*, 1997, doi:10.1029/2003GL017967, 2003.
- Feingold, G., L. A. Remer, J. Ramaprasad, and Y. Kaufman, analysis of smoke impact on clouds in Brazilian biomass burning regions: An extension of Twomey's approach, *J. Geophys. Res.* *106*, 22,907–22,922, 2001.
- Fisch, G., J. Tota, L. A. T. Machado, M. A. F. Silva Dias, R. F. Da F. Lyra, C. A. Nobre, A. J. Dolman, and J. H. C. Gash, The convective boundary layer over pasture and forest in Amazonia, *Theor. Appl. Climatol.*, *78*, 47-59, 2004.
- Golaz, J-C, H. Jiang, and W.R. Cotton, 2001: A Large-eddy simulation study of cumulus clouds over land and sensitivity to soil moisture. *Atmos. Res.*, *59-60*, 373-392.
- Grassl, H, Albedo reduction and radiative heating of clouds by absorbing aerosol particles. Contribution to Atmospheric Physics, Oxford. *48*, 199–210, 1975
- Han, Q., W. B. Rossow, J. Chou, and R. M. Welch, Global survey of the relationships of cloud albedo and liquid water path with droplet size using ISCCP, *J. Climate*, *7*, 1516–1528, 1998.
- Hansen, J., M. Sato, and R. Ruedy, Radiative forcing and climate response. *J. Geophys. Res.* *102*, D6, 6832–6864, 1997.
- Harrington, J. Y., G. Feingold, and W.R. Cotton, Radiative impacts on the growth of a population of drops within simulated summertime Arctic stratus, *J. Atmos. Sci.*, *57*, 766–785, 2000.
- Jacobson M. Z., Control of fossil-fuel particulate black carbon and organic matter, possibly the most effective method of slowing global warming, *J. Geophys. Res.*, *107* (D19), 4410, doi:10.1029/2001JD001376, 2002.

- Jiang, H., G. Feingold, and W. R. Cotton, Simulations of aerosol-cloud-dynamical feedbacks resulting from entrainment of aerosol into the marine boundary layer during the Atlantic Stratocumulus Transition Experiment. *J. Geophys. Res.* *107*, D24, doi:10.1029/2001JD001502, 2002.
- Johnson, B. T., K. P. Shine and P. M. Forster, The semi-direct aerosol effect: Impact of absorbing aerosols on marine stratocumulus, *Q. Jnl. Roy. Meteor. Soc.*, *30*, 1407–1422, 2004.
- Kaufman, Y. J., and T. Nakajima, Effect of Amazon smoke on cloud microphysics and albedo – analysis from satellite imagery. *J. Appl. Meteor.*, *32*, 729–744, 1993.
- Kim B.-G., S. E. Schwartz, M. A. Miller, Q. Min, Effective radius of cloud droplets by ground-based remote sensing: Relationship to aerosol, *J. Geophys. Res.*, *108*, doi:10.1029/2003JD003721, 2003.
- Koren, I., Y.J. Kaufman, L.A. Remer, and J.V. Martins, Measurement of the effect of Amazon smoke on inhibition of cloud formation, *Science*, *303*, 1342–1345, 2004.
- Leaith, W. R., C. M. Banic, G. A. Isaac, M. D. Couture, P. S. K. Liu, I. Gultepe, and S.-M. Li, Physical and chemical observations in marine stratus during the 1993 North Atlantic Regional Experiment: Factors controlling cloud droplet number concentrations, *J. Geophys. Res.*, *101*, 29,123–29,135, 1996.
- Lu, M.-L., and J. H. Seinfeld, Study of the aerosol indirect effect by LES of marine stratocumulus, *J. Atmos. Sci.*, in press, 2005.
- Lohmann, U., and J. Feichter, Global indirect aerosol effects: A review, *Atmos. Chem. Phys.*, *5*, 715–737, 2005.

- Nakajima, T., A. Higurashi, K. Kawamoto, and J. E. Penner, A possible correlation between satellite-derived cloud and aerosol microphysical parameters, *Geophys. Res. Lett.*, *28*, 1171–1174, 2001.
- Nenes, A., R. J. Charlson, M. C. Facchini, M. Kulmala, A. Laaksonen, and J. H. Seinfeld, Can chemical effects on cloud droplet number rival the first indirect effect? *Geophys. Res., Lett.*, *29*, No. 17, 1848, doi:10.1029/2002GL015295, 2002.
- Ramanathan, V., P.J. Crutzen, J. T. Kiehl, and D. Rosenfeld, Aerosols, Climate, and the Hydrological Cycle, *Science*, *294*, 2119–2124, 2001.
- Rosenfeld, D., TRMM observed first direct evidence of smoke from forest fires inhibiting rainfall, *Geophys. Res. Lett.* *26*, 3105, 1999.
- Siebesma, A. P, and co-authors, A large eddy simulation intercomparison study of shallow cumulus convection. *J. Atmos. Sci.*, *60*, 1201–1219, 2003.
- Squires, P., The growth of cloud droplets by condensation. *Aust. J. Sci. Res*, *5*, 66–86., 1952.
- Stevens, B., W. R. Cotton, G. Feingold, and C-H Moeng, Large-eddy simulations of strongly precipitating, shallow, stratocumulus-topped boundary layers, *J. Atmos. Sci.*, *55*, 3616–3638, 1998.
- Stevens, B., and co-authors, Evaluation of large-eddy simulations via observations of nocturnal marine stratocumulus. *Mon. Wea. Rev.*, *133*, 1443–1462, 2004.
- Twomey, S., The nuclei of natural cloud formation, Part II: The supersaturation in natural clouds and the variation of cloud droplet concentration. *Geofis. Pura Appl.*, *43*, 243–249, 1959
- Twomey, S., Pollution and the planetary albedo, *Atmos. Environ.*, *8*, 1251–1256, 1974.

- Tzivion, S., G. Feingold, and Z. Levin, An efficient numerical solution to the stochastic collection equation. *J. Atmos. Sci.*, *44*, 3139–3149, 1987.
- von Randow, C, A. O. Manzi, B. Kruijt, P. J. de Oliveira, F. B. Zanchi, R. L. Silva, M. G. Hodnett, J. H. C. Gash, J. A. Elbers, M. J. Waterloo, F. L. Cardoso, and P. Kabat, Comparative measurements and seasonal variations in energy and carbon exchange over forest and pasture in South West Amazonia, *Theor. Appl. Climatol.*, *78*, 5-26, 2004.
- Walko, R. L., L. E. Band, J. Baron, T. G. F. Kittel, R. Lammers, T. J. Lee, D. Ojima, R. A. Pielke Sr., C. Taylor, C. Tague, C. J. Tremback, and P. L. Vidale, Coupled Atmosphere-biophysics-hydrology models for environmental modeling, *J. appl. meteorol.*, *39*, 931–944, 2000.
- Warner, J., A reduction in rainfall associated with smoke from sugar-cane fires – an inadvertent weather modification? *J. Appl. Meteorol.*, *7*, 247–251, 1968.
- Warner, J., and S. Twomey, The production of cloud nuclei by cane fires and their effect on cloud droplet concentration, *J. Atmos. Sci.*, *24*, 704-706, 1967.
- Xue, Huiwen, and G. Feingold, Large eddy simulations of trade wind cumuli: investigation of aerosol indirect effects. *J. Atmos. Sci.*, 2005, in press.
- Yu H., S. C. Liu, and R. E. Dickinson, Radiative effects of aerosols on the evolution of the atmospheric boundary layer, *J. Geophys. Res.*, *107* (D12), doi:10.1029/2001JD000754, 2002.

Table 1. Description of simulations. N_a is aerosol concentration; τ_a is aerosol optical depth (dry); $\tau_{a,rh}$ is optical depth associated with the hydrated aerosol based on the initial RH profile.

EXP	N_a (cm ⁻³)	τ_a	$\tau_{a,rh}$	Aerosol Heating
S1-100	100	0.04	0.05	No
S1-500	500	0.20	0.26	No
S1-1000	1000	0.40	0.53	No
S1-2000	2000	0.80	1.05	No
S2-100	100			Yes
S2-500	500			Yes
S2-1000	1000			Yes
S2-2000	2000			Yes

Table 2. Comparison of upwelling shortwave (SW) fluxes at the top of atmosphere (TOA) F_{sw}^{\uparrow} (W m^{-2}), and downwelling SW fluxes at the surface F_{sw}^{\downarrow} (W m^{-2}) among all the simulations. Values shown are time averaged over the last 5 h of the simulations.

EXP	F_{sw}^{\uparrow} (TOA)		DIFF	%
N_a	S1	S2	(S2-S1)	(S2-S1)/S1
100	176.9	231.6	54.8	30.9
500	187.1	230.5	43.4	23.2
1000	187.8	239.5	51.7	27.5
2000	191.4	255.1	63.7	33.3
	F_{sw}^{\downarrow} (SFC)		DIFF	%
	S1	S2	(S2-S1)	(S2-S1)/S1
100	740.2	686.0	-54.2	-7.3
500	731.5	663.5	-68.0	-9.3
1000	732.1	621.2	-110.8	-15.1
2000	728.5	535.4	-193.2	-26.5

Table 3. Comparison between simulations using two different values of single scattering albedo $\omega_0 = 0.9$ and $\omega_0 = 1.0$. DIFF is the % difference in fields (relative to $\omega_0 = 1$). Numbers in parentheses are standard deviations.

EXP	R_{net}	$F_{sen+lat}$	LWP	CF	τ_c
ω_0	W m^{-2}	W m^{-2}	g m^{-2}		
0.9	504.1 (96.6)	483.8 (111.7)	126.8 (86.1)	0.147 (0.08)	17.2 (1.6)
1.0	524.6 (94.6)	505.9 (109.4)	163.5 (97.7)	0.174 (0.09)	19.3 (1.7)
% DIFF	3.9	4.3	22.4	15.5	10.8

Both simulations are for $N_a = 1000 \text{ cm}^{-3}$.

Table 4. Correlation coefficients between LWP and $N_{d,int}$, LWP and τ_c , and $N_{d,int}$ and τ_c for S1 simulations.

EXP	Corr(LWP, $N_{d,int}$)	Corr(LWP, τ_c)	Corr($N_{d,int}$, τ_c)
S1-100	0.54	0.87	0.81
S1-500	0.57	0.92	0.71
S1-1000	0.76	0.98	0.86
S1-2000	0.70	0.98	0.81

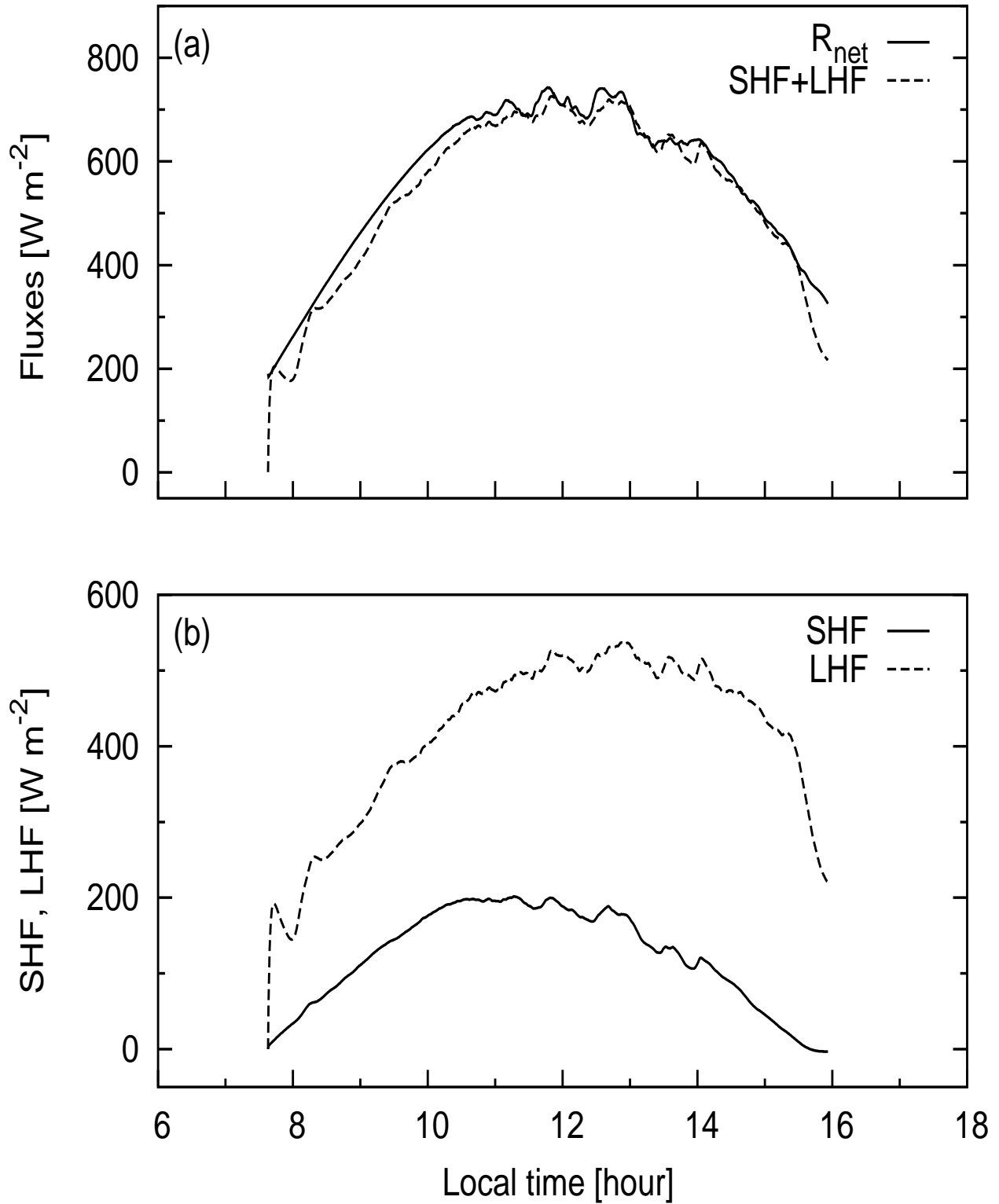


Figure 1. Time series of (a) the modeled net surface radiation and the sum of the surface fluxes and (b) the component surface latent and sensible heat fluxes for the S1-100 simulations

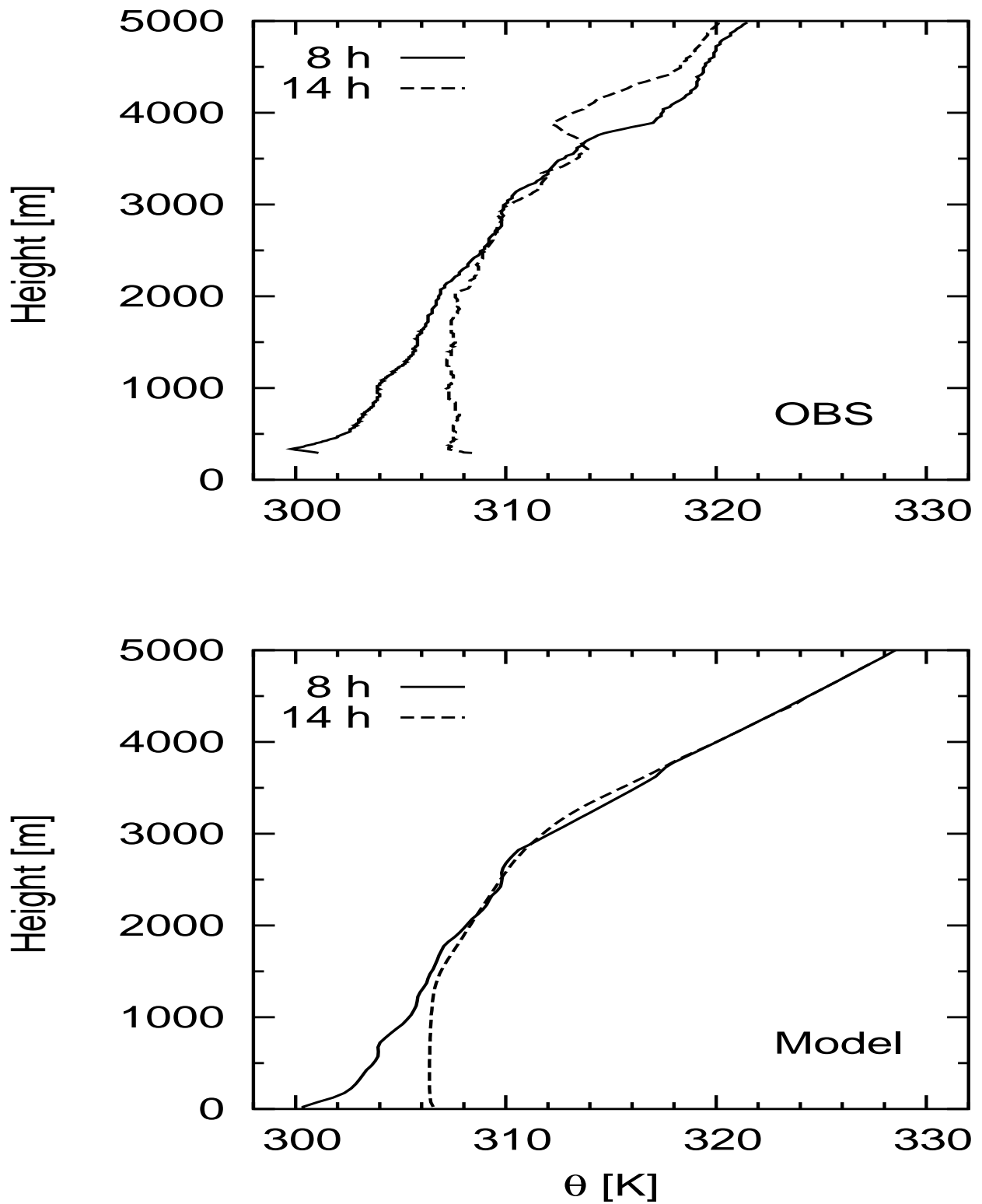


Figure 2. Observed and modeled profiles of potential temperature θ for the S1-100 simulation at 08:00 h and 14:00 h LT.

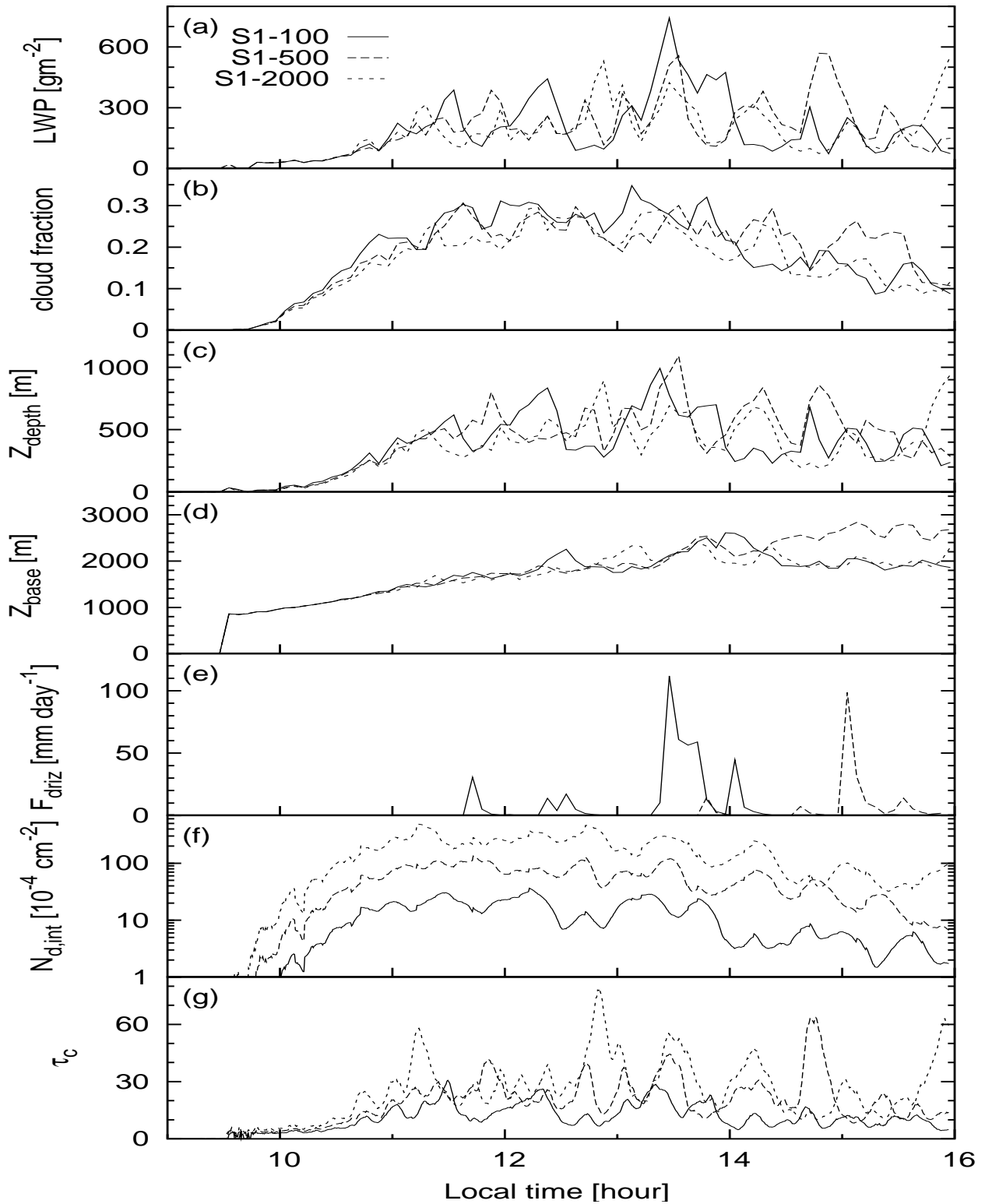


Figure 3. Time series of (a) LWP, (b) cloud fraction, (c) cloud layer depth (Z_{depth}), (d) cloud base Z_{base} , (e) surface drizzle rate (F_{driz}), (f) vertically integrated number concentration of droplets ($N_{d,\text{int}}$), and (g) cloud optical depth (τ_c) for S1 simulations as described

in Table 1. Line types are as labeled.

S u b m i t t e d

October 25, 2005

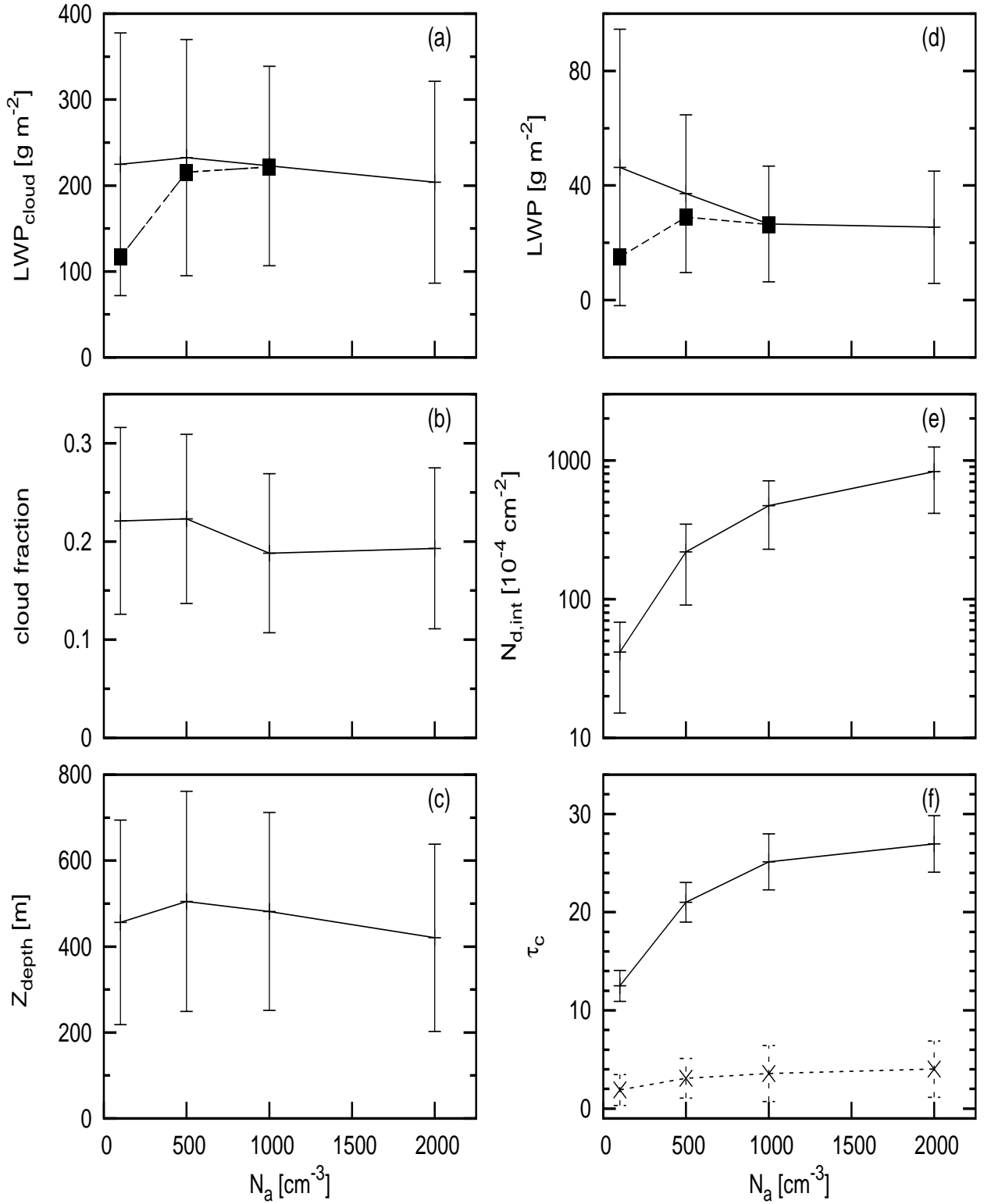


Figure 4. A sample of S1 fields averaged over the last 5 h (11 to 16 LT) of the time series

shown in Figure 3 as a function of aerosol concentrations N_a for S1 simulations. Vertical

lines represent the standard deviation. (a) is LWP averaged over cloudy columns; (d) is

LWP calculated over the entire domain. The filled squares in (a) and (d) are calculations

of the LWP for cloud droplets with radius $\leq 25 \mu\text{m}$.

(f) Calculation of τ_c as a cloud average

(solid line) and a domain average (dashed line). See text for details.

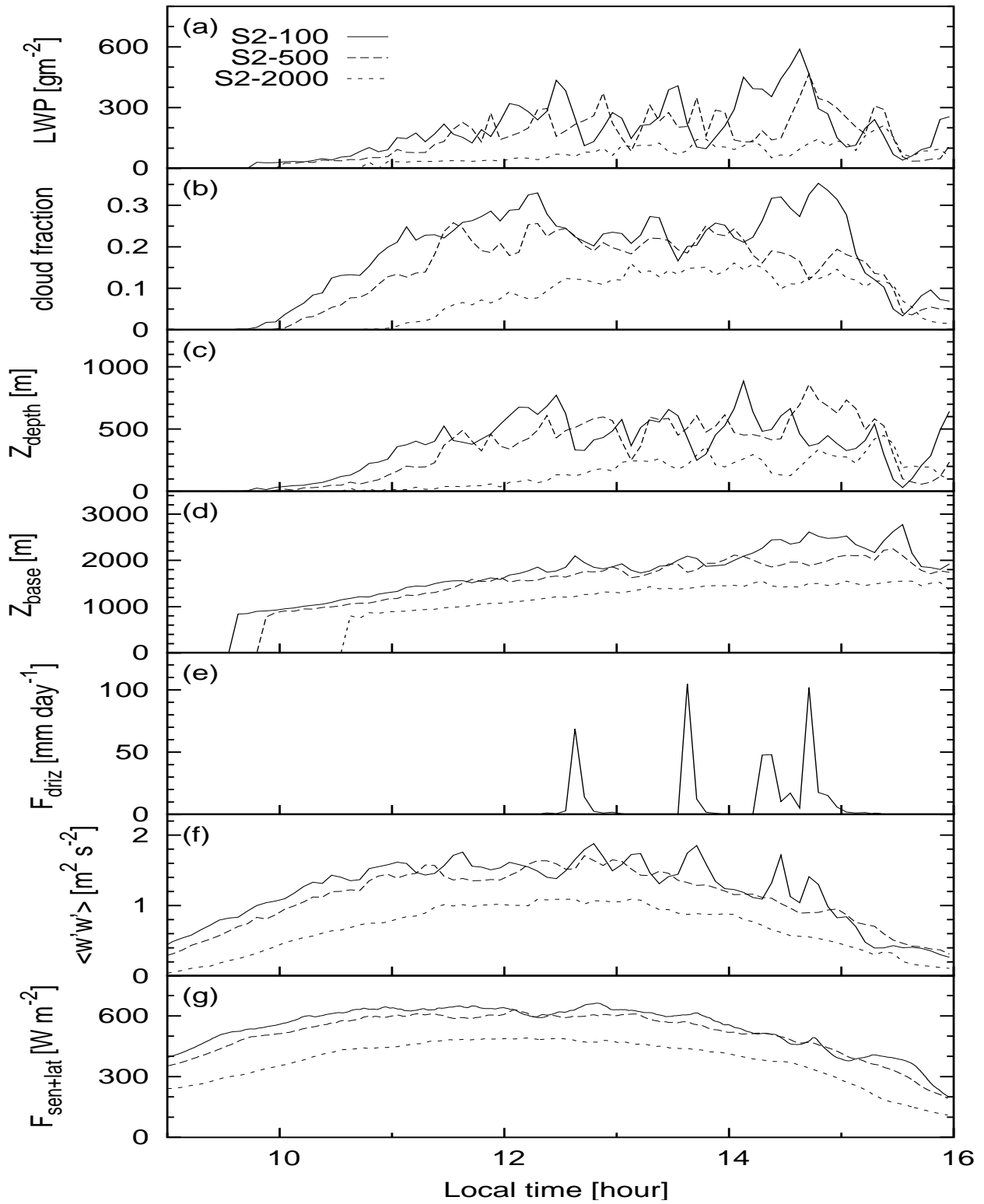


Figure 5. As in Figure 3 but for time series of S2 simulations; (f) is the maximum domain averaged $\langle w'w' \rangle$ which is a measure of convective activity. (g) is the sum of sensible and latent heat fluxes.

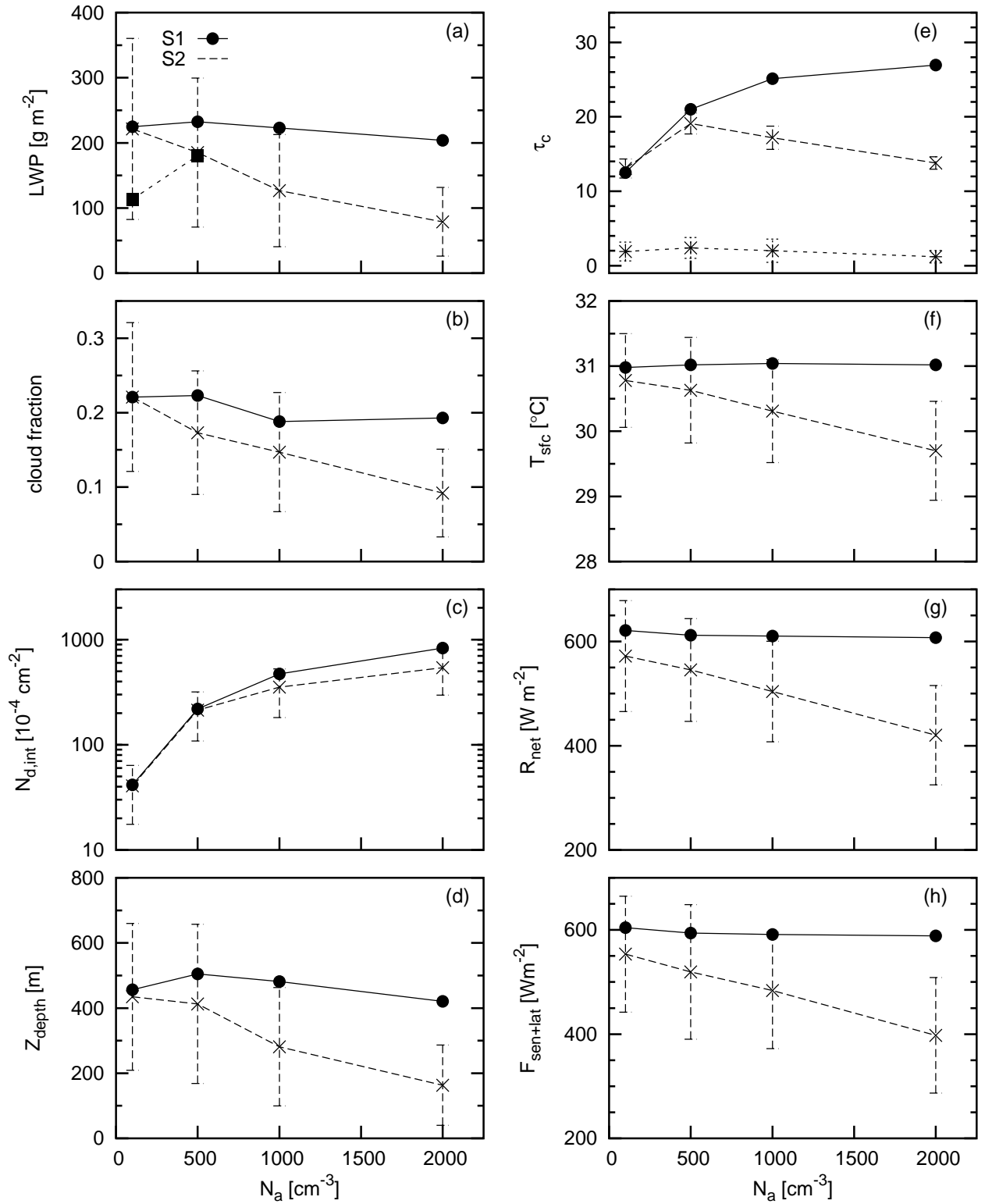


Figure 6. As in Figure 4 but for S2 simulations and an extended set of fields: (a) Square symbols pertain to S2 LWP calculations considering drop sizes $< 25 \mu\text{m}$ radius; (f) Surface temperature T_{sfc} , (g) net surface radiation R_{net} and (h) sum of sensible and latent heat fluxes. S1 results (without standard deviations) are superimposed for comparison.

S u b m i t t e d

October 25, 2005

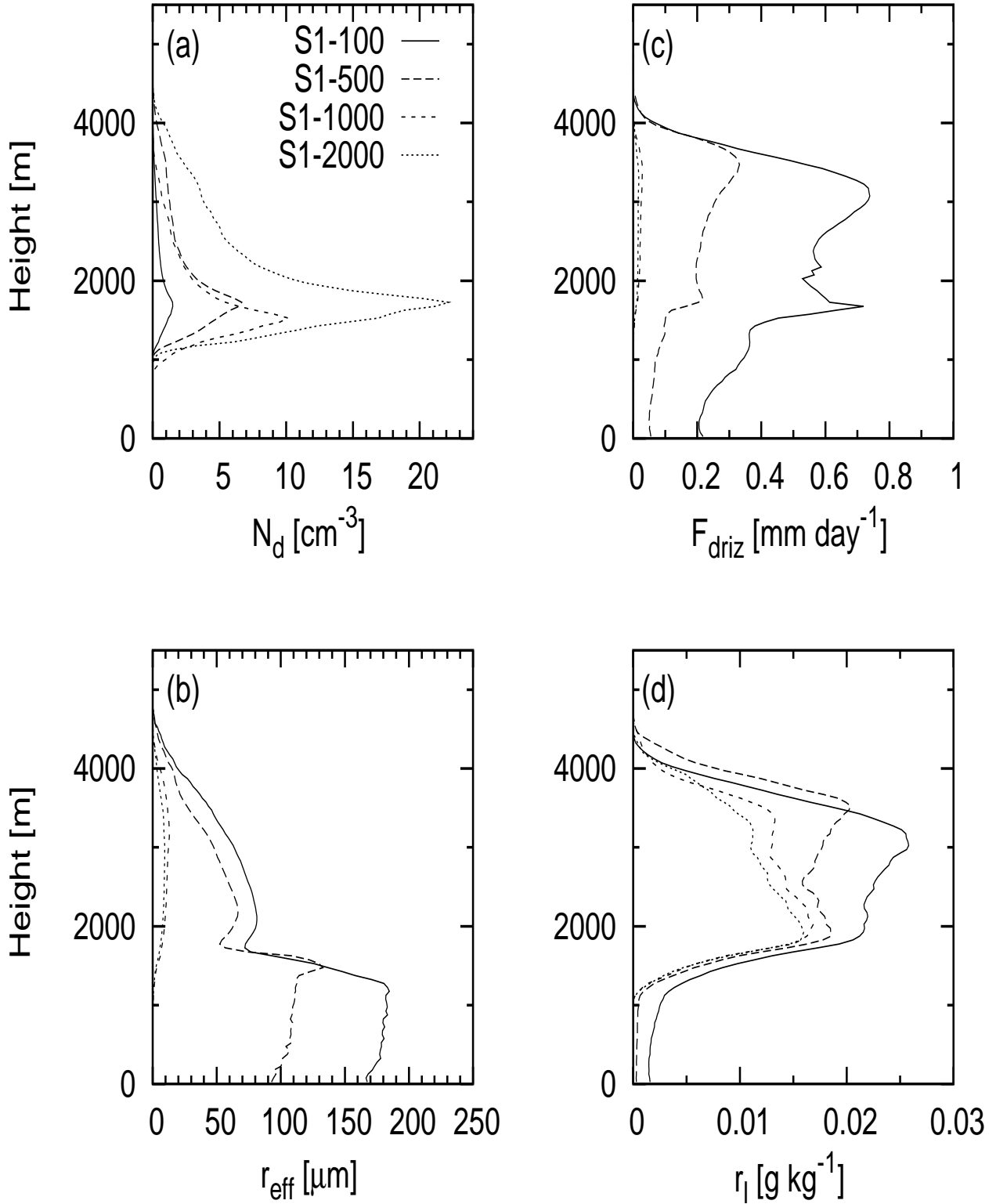


Figure 7. Horizontally averaged profiles of (a) number concentration of droplets (N_d ; domain average), (b) effective radius (r_{eff} ; cloud-average), (c) drizzle rate (F_{driz} ; domain average), and (d) cloud liquid water mixing ratio (r_l ; all drops; domain average), time averaged over the last 5 h (11 to 16 LT) of the S1 simulations. Line types are as indicated.

S u b m i t t e d

October 25, 2005

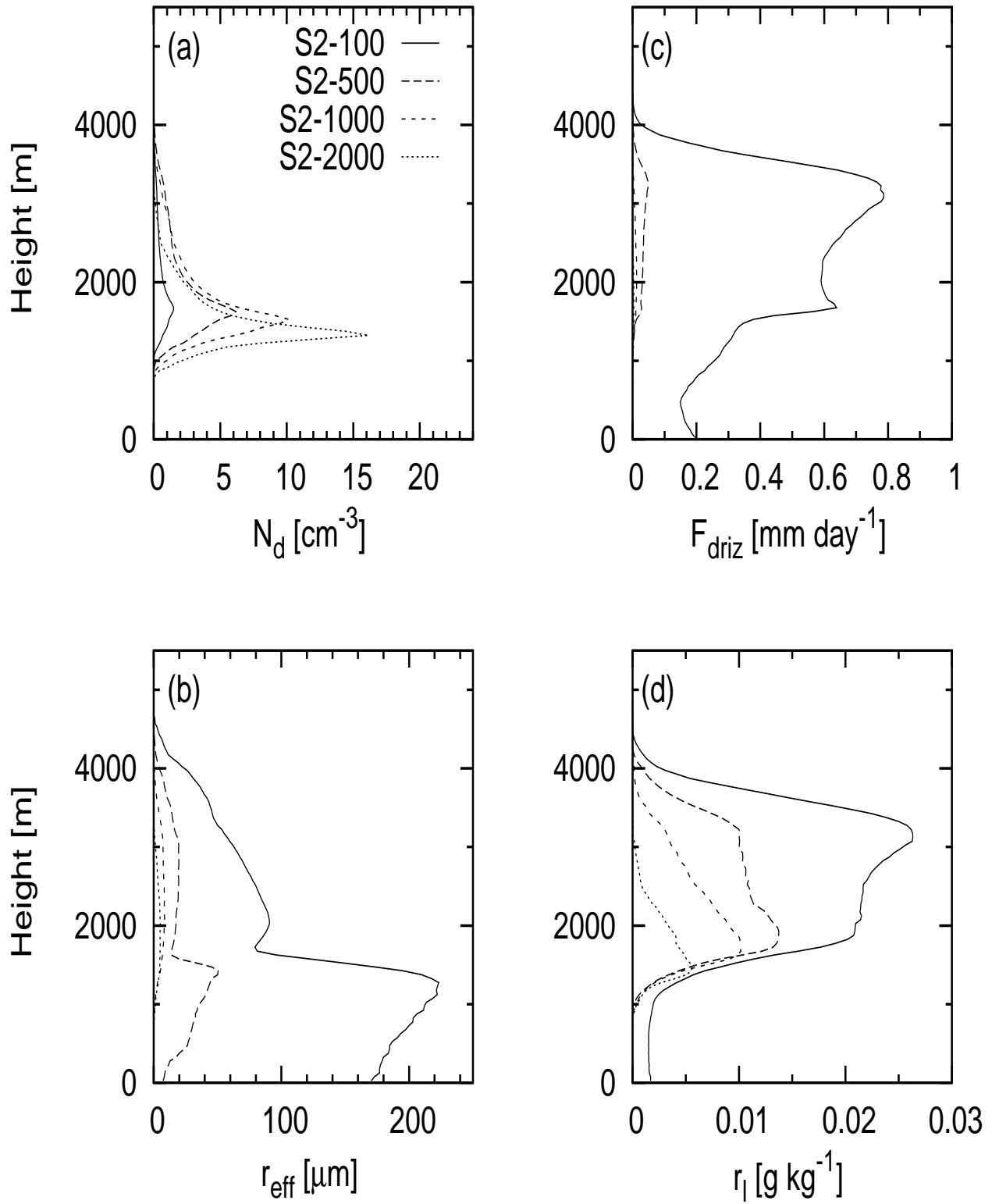


Figure 8. As in Figure 7 but for S2 simulations.

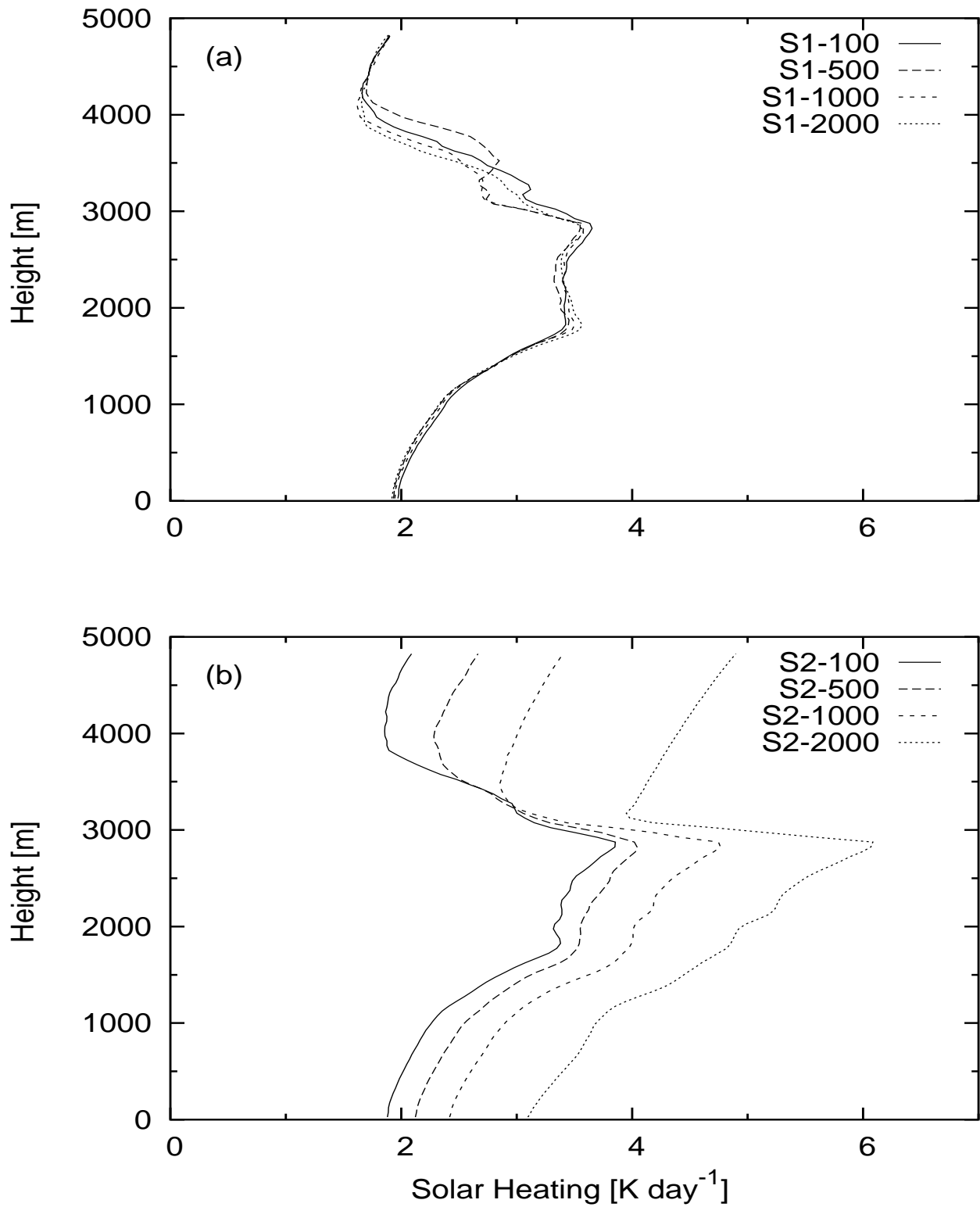


Figure 9. Shortwave radiative heating rates for (a) S1 and (b) S2 simulations. Line types are as indicated.